Laser-assisted electron momentum spectroscopy

Konstantin A. Kouzakov*
Department of Nuclear Physics and Quantum Theory of Collisions, Faculty of Physics, Moscow State University, Moscow 119991, Russia

Yuri V. Popov†
Institute of Nuclear Physics, Moscow State University, Moscow 119991, Russia

Masahiko Takahashi‡
Institute of Multidisciplinary Research for Advanced Materials, Tohoku University, Sendai 980-8577, Japan
(Received 22 April 2010; published 12 August 2010)

We consider theoretically ionization of an atomic target by fast electron impact at large energy and momentum transfer and in the presence of laser radiation. The laser electric-field amplitude is weak compared to the typical field in the target. Two frequency regimes are investigated according to whether the laser frequency is (i) much smaller than or (ii) resonant to the frequency of the transition from the ground to the first excited target state. Fast incident, scattered, and ejected electrons are described using Volkov solutions. The dressing of the bound-electron state by the laser field is accounted for within time-dependent perturbation theory in the case of the low-frequency regime and within the rotating wave approximation in the case of a resonant one. The interaction of the incident electron with the target is treated in the first Born approximation. For atomic hydrogen embedded in a linearly or circularly polarized laser field, we discuss how the polarization-vector orientation influences the momentum-dependent $(e,2e)$ differential cross sections assisted by exchange of few photons between the colliding system and the field. In addition, we inspect the dependence of the cross sections on the dressing of the hydrogen state.

DOI: 10.1103/PhysRevA.82.023410 PACS number(s): 34.80.Qb, 34.80.Dp

I. INTRODUCTION

More than 40 years ago Smirnov and Neudatchin proposed to use the $(e,2e)$ method for measurement of electron-momentum distribution in matter [1]. Since then the method has developed into a powerful tool for exploring the electronic structure of various systems ranging from atoms [2,3] and molecules [4] to clusters [5] and solids [6]. In the literature it is often referred to as electron momentum spectroscopy (EMS) (see Refs. [7–10] and references therein). The key feature of EMS is the kinematics of quasielastic knock-out of the target electron by the fast incoming electron at large energy and momentum transfer. This is realized under the so-called high-energy Bethe ridge conditions, when the energy and momentum transferred to the target are absorbed by the ejected electron. Describing the fast incoming and outgoing electrons by plane waves and involving the Born approximation (in this connection see Ref. [11]), one obtains the coincident differential cross section which is proportional to the one-electron momentum density $|\psi(\mathbf{q})|^2$ of the ionized electron orbital. The shape of the cross section as a function of kinematic variables depends strongly only on $\mathbf{q}$ and therefore it is usually called the momentum profile [9].

Recently, the first kinematically complete $(e,2e)$ measurements in the presence of a laser field were realized [12]. The experiment was performed on the helium atom at an impact energy of 1 keV and in the so-called asymmetric kinematics involving small energy and momentum transfer. The laser radiation with the photon energy $\hbar\omega = 1.17$ eV and the intensity $I = 4 \times 10^{12}$ W/cm^2 was by itself insufficient to produce any appreciable ionizing effect. This ensures that the ionization yield was produced due to electron-helium collisions. The measured $(e,2e)$ cross sections demonstrated marked differences as compared to the field-free analogs. This notable advance in experimental studies on electron-impact ionization indicates that the first laser-assisted EMS measurements are feasible in the near future. Therefore a corresponding theoretical consideration becomes desirable.

A number of theoretical works on laser-assisted $(e,2e)$ collisions in atomic systems have been published so far. Some overview of these works can be found in Mittleman [13] and two review articles [14,15]. To our knowledge, all the published studies deal with the case of kinematics that involves small energy and momentum transfer. Such a situation is unsurprising because historically this type of $(e,2e)$ kinematics is much more often investigated, both experimentally and theoretically, than that of EMS. Let us briefly summarize the main theoretical findings concerning the laser-field effect on the coincident differential cross sections. First, the cross sections are seriously modified even by the presence of low-intensity laser radiation. Second, they strongly depend on the dressing of the atomic target states. The latter finding is especially interesting from the viewpoint of perspectives of laser-assisted EMS. Indeed, the EMS is known to be very informative about the target electron states and hence one might expect that it is able to provide valuable information on the field-dressed target states as well.

The purpose of the present work is twofold: (i) to deliver a theoretical consideration of the laser-assisted EMS and (ii) to examine the potential of the method for exploring laser-modified electron-momentum distributions in atomic systems.

*kouzakov@srd.sinp.msu.ru
†popov@srd.sinp.msu.ru
‡masahiko@tagen.tohoku.ac.jp

Our theoretical analysis is performed for laser electric-field amplitudes that are much weaker than the intra-atomic field. Two physically distinct frequency regimes are in focus. In the first regime, the laser frequency is well below the frequency required to induce one-photon transitions from the ground target state. The dressing of the target states in this case is adequately described within time-dependent perturbation theory. In the second regime, the laser frequency is resonant to the transition from the ground to the first excited target state. This case of laser parameters allows one to treat the target as a two-level system and solve the laser-target interaction problem in a nonperturbative fashion. The theory developed for both frequency regimes is illustrated below with numerical examples in the case of an archetypical target, namely, the hydrogen atom.

The article is organized as follows. In Sec. II, we formulate the S matrix for the EMS method when the laser field is present and derive the coincident differential cross sections using several models of the field-dressed target state. Numerical results for the laser-assisted momentum profiles from atomic hydrogen are discussed in Sec. III. The role of the polarization-vector direction is analyzed for both linearly and circularly polarized laser fields. The conclusions are drawn in Sec. IV. Atomic units (a.u., $e = \hbar = m_e = 1$) are used throughout unless otherwise stated.

II. THEORY

We consider the process where, in the presence of a laser field, a fast electron impinges on an atomic target and induces $(e,2e)$ collision at high impact energy and large momentum transfer. As a result, a fast outgoing electron pair emerges which is formed by the scattered and ejected electrons. The target is supposed to have only one active electron that participates in the laser-assisted $(e,2e)$ collision. In what follows, the incident, scattered, and ejected electron energies and momenta are specified respectively by $(E_0,\mathbf{p}_0)$, $(E_s,\mathbf{p}_s)$, and $(E_e,\mathbf{p}_e)$.

A. Laser field

The laser field is assumed to switch on and off adiabatically at $t \to -\infty$ and $t \to +\infty$, respectively. More specifically, the turn on and off time δT of the laser pulse as well as the laser pulse duration T are very long on a time scale typical for the target and much longer than the collision duration. We consider the case of a monochromatic elliptically polarized laser wave with frequency ω and a wave vector $\mathbf{k}$ ($k = \omega/c$). Without loss of generality we suppose that the z axis is directed along $\mathbf{k}$. A typical situation is when the laser wavelength $\lambda = 2\pi/k$ is much greater than the spatial extent both of the target and of the region where the electron-electron collision takes place. This validates the use of the dipole approximation for the electric component of the laser field:

$$\boldsymbol{\mathcal{E}}(t) = \mathcal{E}_x \hat{\mathbf{e}}_x \cos\omega t + \mathcal{E}_y \hat{\mathbf{e}}_y \sin\omega t, \tag{1}$$

where $\mathcal{E}_x > 0$ and $\mathcal{E}_y > 0$ ($\mathcal{E}_y < 0$) for right (left) polarization. As remarked in Sec. I, the present study deals with situations in which the electric-field amplitude $\mathcal{E}_0 = \sqrt{\mathcal{E}_x^2 + \mathcal{E}_y^2}$ is much less than the typical field in the target $\mathcal{E}_T$. The vector potential corresponding to (1) is

$$\mathbf{A}(t) = A_x \hat{\mathbf{e}}_x \sin\omega t + A_y \hat{\mathbf{e}}_y \cos\omega t, \tag{2}$$

with $A_x = -c\mathcal{E}_x/\omega$ and $A_y = c\mathcal{E}_y/\omega$. Note that the case of linear polarization derives from (1) on setting $\mathcal{E}_x = \mathcal{E}_0$ and $\mathcal{E}_y = 0$, while that of circular polarization amounts to $\mathcal{E}_x = |\mathcal{E}_y| = \mathcal{E}_0/\sqrt{2}$.

B. S matrix

In the field-free case, the collision mechanism under the kinematical conditions of EMS is as follows. The incoming electron knocks out a bound electron from the target, transferring a large amount of its energy and momentum to the ejected electron. An important feature is that the value of the momentum

$$\mathbf{q} = \mathbf{p}_s + \mathbf{p}_e - \mathbf{p}_0, \tag{3}$$

which is opposite to the recoil momentum of the ionized target, is very small compared to the values of the incoming and outgoing electron momenta. Another important feature is that the incoming and outgoing electron energies are high enough to describe all the asymptotically free electrons by plane waves. Under these circumstances, the $(e,2e)$ process closely resembles collision of two free electrons with initial momenta $\mathbf{p}_0,\mathbf{q}$ and final momenta $\mathbf{p}_s,\mathbf{p}_e$. The scattering amplitude is therefore appropriately evaluated within the plane wave Born approximation (PWBA) framework which treats the process to the lowest order in the interaction between the colliding electrons. The presence of a laser field does not affect the electron-electron interaction responsible for the $(e,2e)$ transition but it modifies both the free- and the bound-electron states. Summarizing the above remarks, the S matrix for the laser-assisted $(e,2e)$ collision in the kinematical regime of EMS is given by the expression

$$S = -i \int_{-\infty}^{\infty} dt \left\langle \chi_{\mathbf{p}_s}(\mathbf{r}_0,t)\chi_{\mathbf{p}_e}(\mathbf{r}_1,t) \left| \frac{1}{r_{01}} \right| \chi_{\mathbf{p}_0}(\mathbf{r}_0,t)\psi_T(\mathbf{r}_1,t) \right\rangle, \tag{4}$$

where $r_{01} = \mathbf{r}_0 - \mathbf{r}_1 \cdot \chi_{\mathbf{p}}(\mathbf{r},t)$ is a nonrelativistic Volkov wave [16] describing the motion of the free electron under the action of the laser field. $\psi_T(\mathbf{r}_1,t)$ is a wave function of the target electron state dressed by the laser field.

C. Free-electron states

The Volkov wave solves the following Schrödinger equation:

$$i\frac{\partial}{\partial t}\chi_{\mathbf{p}}(\mathbf{r},t) = H_F \chi_{\mathbf{p}}(\mathbf{r},t), \tag{5}$$

where[1]

$$H_F = \frac{1}{2}\left(\hat{\mathbf{p}} + \frac{1}{c}\mathbf{A}(t)\right)^2 \tag{6}$$

[1]Hereafter we use the velocity gauge.

is the free-electron Hamiltonian in the presence of the laser field. For the vector potential given by (2) we have (see, for instance, Ref. [17])

$$\chi_{\mathbf{p}}(\mathbf{r},t) = \exp\{i[\mathbf{p}\cdot\mathbf{r} - \gamma\sin(\omega t+\delta) - Et - \zeta(t)]\}, \quad (7)$$

where $E = p^2/2$ and

$$\gamma = \frac{\sqrt{\mathcal{E}_x^2 p_x^2 + \mathcal{E}_y^2 p_y^2}}{\omega^2}, \quad \delta = \arcsin\left(\frac{\mathcal{E}_x p_x}{\sqrt{\mathcal{E}_x^2 p_x^2 + \mathcal{E}_y^2 p_y^2}}\right),$$

$$\zeta(t) = \frac{1}{2c^2}\int_{-\infty}^{t} A^2(t')dt'.$$

D. Bound-electron states

The target wave function is a solution to the time-dependent Schrödinger equation

$$i\frac{\partial}{\partial t}\psi_T(\mathbf{r}_1,t) = H_T\psi_T(\mathbf{r}_1,t), \quad (8)$$

where

$$H_T = \frac{1}{2}\left(\hat{\mathbf{p}}_1 + \frac{1}{c}\mathbf{A}(t)\right)^2 + V(\mathbf{r}_1) \quad (9)$$

is the Hamiltonian of the target in the presence of the laser field. It is usual to seek a solution to Eq. (8) in the form of the expansion

$$\psi_T(\mathbf{r}_1,t) = \sum_n a_n(t)e^{-iE_n t}\psi_n(\mathbf{r}_1), \quad (10)$$

where E_n and ψ_n are eigenenergies and eigenstates of the target Hamiltonian in the absence of the laser field. The target state (10) satisfies the boundary condition

$$\psi_T(\mathbf{r}_1, t\to-\infty) \to \exp(-iE_g t)\psi_g(\mathbf{r}_1),$$

where E_g and $\psi_g(\mathbf{r}_1)$ are the energy and wave function of the undressed ground state of the target.

1. Low-frequency regime

Let us consider the situation when $\omega \ll \omega_{fg} = E_f - E_g$, where E_f is the energy of the first excited target state. This means that the laser field can induce only multiphoton transitions from the ground target state. The probability of such transitions is very low due to the weakness of the field. Under these circumstances, it is relevant to treat the time-dependent interaction in the Hamiltonian (9),

$$W(t) = \frac{1}{c}\mathbf{A}(t)\cdot\hat{\mathbf{p}}_1 + \frac{1}{2c^2}A^2(t),$$

as perturbation, when describing the laser influence on the target states.

The gauge transformation $a_n \to \exp[-i\zeta(t)]a_n$ removes from the target Hamiltonian (9) the term quadratic in the vector potential and the time-dependent perturbation treatment can be developed in $W(t) = \mathbf{A}(t)\cdot\hat{\mathbf{p}}_1/c$. In particular, such an approach was adopted in the theoretical studies on laser-assisted ionization of one-electron atoms and ions upon charged-particle impact involving small energy and momentum transfer [18]. The first order of the time-dependent perturbation theory yields the field-dressed target state (10) as

$$\psi_T(\mathbf{r}_1,t) = \exp\{-i[E_g t + \zeta(t)]\}\left[\psi_g(\mathbf{r}_1) + \frac{1}{2i\omega}\right.$$
$$\times\sum_{n\neq g}\left(e^{i\omega t}\frac{\langle n|\mathcal{E}_x\hat{p}_{1,x} - i\mathcal{E}_y\hat{p}_{1,y}|g\rangle}{\omega_{ng}+\omega}\right.$$
$$\left.\left. - e^{-i\omega t}\frac{\langle n|\mathcal{E}_x\hat{p}_{1,x} + i\mathcal{E}_y\hat{p}_{1,y}|g\rangle}{\omega_{ng}-\omega}\right)\psi_n(\mathbf{r}_1)\right], \quad (11)$$

where $\omega_{ng} = E_n - E_g$. Since $\omega_{ng} \gg \omega$, we may use in Eq. (11) the low-frequency approximation $\omega_{ng} \pm \omega \approx \omega_{ng}$. This yields (see Ref. [19] for detail)

$$\psi_T(\mathbf{r}_1,t) = \exp\{-i[E_g t + \zeta(t)]\}$$
$$\times\left(1 + \frac{i}{\omega}(\mathcal{E}_x x_1\sin\omega t - \mathcal{E}_y y_1\cos\omega t)\right)\psi_g(\mathbf{r}_1). \quad (12)$$

An alternative perturbation approach was employed in the theoretical works devoted to the laser-assisted $(e,2e)$ reactions in atomic hydrogen [20] and helium [21] in asymmetric coplanar geometry at small energy and momentum transfer. After transforming in Eq. (10) from the velocity to the length gauge, $a_n \to \exp[-i\mathbf{A}(t)\cdot\mathbf{r}_1/c]a_n$, one is left with the perturbation interaction $W(t) = \boldsymbol{\mathcal{E}}(t)\mathbf{r}_1$ in the Hamiltonian. Developing the time-dependent perturbation theory to first order, one obtains

$$\psi_T(\mathbf{r}_1,t) = \exp(-iE_g t)\exp\left(-\frac{i}{c}\mathbf{A}(t)\cdot\mathbf{r}_1\right)$$
$$\times\left[\psi_g(\mathbf{r}_1) - \frac{1}{2}\sum_{n\neq g}\left(e^{i\omega t}\frac{\langle n|\mathcal{E}_x x_1 - i\mathcal{E}_y y_1|g\rangle}{\omega_{ng}+\omega}\right.\right.$$
$$\left.\left. + e^{-i\omega t}\frac{\langle n|\mathcal{E}_x x_1 + i\mathcal{E}_y y_1|g\rangle}{\omega_{ng}-\omega}\right)\psi_n(\mathbf{r}_1)\right]. \quad (13)$$

Equation (13) is simplified by employing low-energy and closure approximations (see, for instance, Ref. [22]):

$$\psi_T(\mathbf{r}_1,t) = \exp(-iE_g t)\exp\left[-\frac{i}{c}\mathbf{A}(t)\cdot\mathbf{r}_1\right]$$
$$\times\left(1 - \frac{1}{\omega_{\rm cl}}(\mathcal{E}_x x_1\cos\omega t + \mathcal{E}_y y_1\sin\omega t)\right)\psi_g(\mathbf{r}_1), \quad (14)$$

where $\omega_{\rm cl} \gg \omega$ is a "mean" target transition frequency (the closure parameter).

Finally, the zeroth-order approximation to the solution of Eq. (8), that is, the approach which was utilized in the early theoretical studies on laser-assisted electron-atom ionizing collisions (see, for instance, Refs. [23]), is given by the field-free target state

$$\psi_T(\mathbf{r}_1,t) = \exp(-iE_g t)\psi_g(\mathbf{r}_1). \quad (15)$$

2. *Resonant regime*

When the laser frequency is close to or coincides with $\omega_{fg} = E_f - E_g$, the main contribution to the field-dressed wave function (10) is provided by the ground and first excited target states. Therefore we can write down

$$\psi_T(\mathbf{r}_1,t) = e^{-iE_g t}a_g(t)\psi_g(\mathbf{r}_1) + e^{-iE_f t}\sum_v a_{f_v}(t)\psi_{f_v}(\mathbf{r}_1), \tag{16}$$

where we have accounted for degeneracy of the excited state. The expansion coefficients are found by substituting the ansatz (16) in Eq. (8), projecting the left and right parts of the Schrödinger equation onto the field-free states ψ_n $(n = g, f_v)$ and then solving the resultant system of differential equations. The latter can be done using the so-called rotating wave approximation (RWA) [13] which neglects the fast-oscillating terms $\propto e^{\pm i(\omega_{fg}+\omega)t}$ and $\propto e^{\pm i\omega t}$ in comparison with the slow-oscillating terms $\propto e^{\pm i(\omega_{fg}-\omega)t}$. This procedure yields

$$\begin{aligned} a_g^{\pm}(t) &= \sqrt{\frac{|\Delta|+\Omega}{2\Omega}}\exp[-i\zeta(t)]\exp\left(-\frac{i}{2}(\Delta\mp\Omega)t\right), \\ a_{f_v}^{\pm}(t) &= \mp\frac{\sqrt{2}\mathcal{M}_{f_v,g}}{\sqrt{\Omega(|\Delta|+\Omega)}}\exp[-i\zeta(t)]\exp\left(\frac{i}{2}(\Delta\pm\Omega)t\right). \end{aligned} \tag{17}$$

Here

$$\mathcal{M}_{f_v,g} = \frac{\omega_{fg}}{2\omega}\langle f_v|\mathcal{E}_x x_1 + i\mathcal{E}_y y_1|g\rangle$$

and

$$\Delta = \omega_{fg} - \omega, \quad \Omega = \sqrt{\Delta^2 + \chi_{f,g}^2} \tag{18}$$

are the resonance detuning and the generalized Rabi frequency, respectively, while

$$\chi_{f,g} = 2\sqrt{\sum_v |\mathcal{M}_{f_v,g}|^2}$$

stands for the Rabi frequency. Note that according to Eq. (17) the following relations hold true:

$$\begin{aligned} |a_g^{\pm}(t)|^2 + \sum_v |a_{f_v}^{\pm}(t)|^2 = 1, \quad |a_g^{\pm}(t)|^2 \geqslant \frac{1}{2}, \\ \sum_v |a_{f_v}^{\pm}(t)|^2 \leqslant \frac{1}{2}. \end{aligned} \tag{19}$$

The field-dressed target state is thus given by

$$\begin{aligned} \psi_T^{\pm}(\mathbf{r}_1,t) = \exp\left[-i\left(E_g t + \frac{1}{2}(\Delta\mp\Omega)t + \zeta(t)\right)\right]\sqrt{\frac{|\Delta|+\Omega}{2\Omega}} \\ \times\left(\psi_g(\mathbf{r}_1) \mp e^{-i\omega t}\sum_v \frac{2\mathcal{M}_{f_v,g}}{|\Delta|+\Omega}\psi_{f_v}(\mathbf{r}_1)\right). \end{aligned} \tag{20}$$

The target wave function evolves into $\psi_T^+(\mathbf{r}_1,t)$ or $\psi_T^-(\mathbf{r}_1,t)$ according to whether $\Delta \geqslant 0$ or $\Delta < 0$.

E. Differential cross sections

In this subsection we derive fully and tripley differential cross sections (FDCS and TDCS) for the models of the field-dressed target state presented above. These are given by Eqs. (12), (14), (15), and (20). In deriving the cross sections, the following formulas are employed [24]:

$$e^{iz\sin\xi} = \sum_{l=-\infty}^{\infty} J_l(z)e^{il\xi}, \quad J_l(z) = \frac{i^{-l}}{\pi}\int_0^{\pi} d\xi\, e^{iz\cos\xi}\cos(l\xi),$$

where J_l is a Bessel function of integer order. These formulas allow us to write down

$$\begin{aligned} &\exp\left(-\frac{i}{c}\mathbf{A}(t)\mathbf{r}\right) \\ &= \exp\left(\frac{i}{\omega}\mathcal{E}_x x\sin\omega t\right)\exp\left(-\frac{i}{\omega}\mathcal{E}_y y\cos\omega t\right) \\ &= \frac{1}{\pi^2}\sum_{l,l'=-\infty}^{\infty} e^{i(l+l')\omega t} i^{-l}\int_0^{\pi} d\xi\int_0^{\pi} d\xi'\cos(l\xi)\cos(l'\xi') \\ &\quad\times\exp\left(\frac{i}{\omega}(\mathcal{E}_x x\cos\xi - \mathcal{E}_y y\cos\xi')\right) \\ &= \sum_{L=-\infty}^{\infty} e^{iL\omega t} i^{L}\int_0^{2\pi}\frac{d\xi}{2\pi} \\ &\quad\times\exp\left[i\left(L\xi - \frac{1}{\omega}(\mathcal{E}_x x\cos\xi - \mathcal{E}_y y\sin\xi)\right)\right]. \end{aligned} \tag{21}$$

1. *The case of (12)*

Inserting solutions (7) and (12) into Eq. (4), we get

$$S = -\frac{4i\pi}{|\mathbf{p}_0 - \mathbf{p}_s|^2}\sum_{N=-\infty}^{\infty} 2\pi\delta(E_s + E_e - E_0 - E_g + N\omega)\mathcal{F}_N(\mathbf{q}), \tag{22}$$

where the function $\mathcal{F}_N(\mathbf{q})$ is given by

$$\begin{aligned} \mathcal{F}_N(\mathbf{q}) = e^{iN\varphi}\left[J_N(\alpha) + J_{N-1}(\alpha)\frac{e^{-i\varphi}}{2\omega}\left(\mathcal{E}_y\frac{\partial}{\partial q_y} + i\mathcal{E}_x\frac{\partial}{\partial q_x}\right)\right. \\ \left. + J_{N+1}(\alpha)\frac{e^{i\varphi}}{2\omega}\left(\mathcal{E}_y\frac{\partial}{\partial q_y} - i\mathcal{E}_x\frac{\partial}{\partial q_x}\right)\right]\psi_g(\mathbf{q}), \end{aligned} \tag{23}$$

with

$$\alpha = \frac{\sqrt{\mathcal{E}_x^2 q_x^2 + \mathcal{E}_y^2 q_y^2}}{\omega^2}, \quad e^{i\varphi} = \frac{\mathcal{E}_y q_y + i\mathcal{E}_x q_x}{\sqrt{\mathcal{E}_x^2 q_x^2 + \mathcal{E}_y^2 q_y^2}},$$

$$\psi_g(\mathbf{q}) = \int d\mathbf{r}_1 e^{-i\mathbf{q}\cdot\mathbf{r}_1}\psi_g(\mathbf{r}_1),$$

and the momentum $\mathbf{q}$ as defined in (3). It should be noted that in the field-free case the function (23) reduces to $\mathcal{F}_N(\mathbf{q}) = \delta_{N0}\psi_g(\mathbf{q})$. If the target is a hydrogenlike ion with nuclear charge Z $(g = 1s)$, Eq. (23) gives

$$\begin{aligned} \mathcal{F}_N(\mathbf{q}) &= \sqrt{\frac{Z^3}{\pi}}\frac{8\pi Z(q^2 + Z^2 - 4N\omega)}{(q^2+Z^2)^3}e^{iN\varphi}J_N(\alpha) \\ &= i^N\sqrt{\frac{Z^3}{\pi}}\frac{4Z(q^2 + Z^2 - 4N\omega)}{(q^2+Z^2)^3} \\ &\quad\times\int_0^{2\pi} d\xi\exp\{i[N\xi - \alpha\cos(\xi-\varphi)]\}, \end{aligned} \tag{24}$$

where we have used the recurrence relation [24]

$$J_{N-1}(z) + J_{N+1}(z) = \frac{2N}{z} J_N(z).$$

On the basis of (22) we can present the FDCS as

$$\frac{d^4\sigma}{dE_s dE_e d\Omega_s d\Omega_e} = \sum_{N=-\infty}^{\infty} d^3\sigma_N \delta(E_s + E_e - E_0 - E_g + N\omega), \tag{25}$$

where the TDCS or momentum profile corresponding to absorption ($N < 0$) or emission ($N > 0$) of N photons by the colliding system is given by

$$d^3\sigma_N = \frac{p_s p_e}{(2\pi)^3 p_0} \left(\frac{d\sigma}{d\Omega}\right)_{ee} |\mathcal{F}_N(\mathbf{q})|^2. \tag{26}$$

Here

$$\left(\frac{d\sigma}{d\Omega}\right)_{ee} = \frac{4}{|\mathbf{p}_0 - \mathbf{p}_s|^4} \left(1 + \frac{|\mathbf{p}_0 - \mathbf{p}_s|^4}{|\mathbf{p}_0 - \mathbf{p}_e|^4} - \frac{|\mathbf{p}_0 - \mathbf{p}_s|^2}{|\mathbf{p}_0 - \mathbf{p}_e|^2}\right) \tag{27}$$

is the half-off-shell Mott-scattering cross section that takes account of exchange between the colliding electrons.

2. The case of (14)

Substituting the target state (14) in Eq. (4), the FDCS can be presented as

$$\frac{d^4\sigma}{dE_s dE_e d\Omega_s d\Omega_e} = \sum_{N=-\infty}^{\infty} d^3\sigma_N \delta(E_s + E_e + U_p - E_0 - E_g + N\omega), \tag{28}$$

where

$$U_p = \frac{\mathcal{E}_0^2}{4\omega^2} \tag{29}$$

is the ponderomotive energy. The momentum profile in Eq. (28) has the same form as (26), with, however [cf. Eq. (23)],

$$\mathcal{F}_N(\mathbf{q}) = i^N \int_0^{2\pi} \frac{d\xi}{2\pi} \exp\{i[N\xi - \alpha\cos(\xi - \varphi) - \beta\sin(2\xi)]\} \times \left[1 + \frac{i}{\omega_{\rm cl}}\left(\mathcal{E}_x \sin\xi \frac{\partial}{\partial q_x} + \mathcal{E}_y \cos\xi \frac{\partial}{\partial q_y}\right)\right] \times \psi_g\left(\mathbf{q} + \mathbf{e}_x \frac{\mathcal{E}_x}{\omega}\cos\xi - \mathbf{e}_y \frac{\mathcal{E}_y}{\omega}\sin\xi\right), \tag{30}$$

where

$$\beta = \frac{\mathcal{E}_x^2 - \mathcal{E}_y^2}{8\omega^3}. \tag{31}$$

When the target is a hydrogenlike ion with nuclear charge Z, we derive

$$\mathcal{F}_N(\mathbf{q}) = i^N \sqrt{\frac{Z^3}{\pi}} \int_0^{2\pi} d\xi \frac{4Z\exp\{i[N\xi - \alpha\cos(\xi - \varphi) - \beta\sin(2\xi)]\}}{[q^2 + Z^2 + 2U_p - 2\alpha\omega\sin(\xi - \varphi) + 4\beta\omega\cos(2\xi)]^3} \times \left[q^2 + Z^2 + 2U_p - 2\alpha\omega\left(\sin(\xi - \varphi) + 2i\frac{\omega}{\omega_{\rm cl}}\cos(\xi - \varphi)\right) + 4\beta\omega\left(\cos(2\xi) - 4i\frac{\omega}{\omega_{\rm cl}}\sin(2\xi)\right)\right]. \tag{32}$$

Here the closure parameter can be estimated as $\omega_{\rm cl} \sim Z^2/2$. Since $\omega \ll \omega_{21}$, where $\omega_{21} = E_{2p} - E_{1s} = 3Z^2/8$, the terms proportional to the ratio $\omega/\omega_{\rm cl}$ bring only a minor correction to $\mathcal{F}_N(\mathbf{q})$.

3. The case of (15)

This case differs from the previous one in (30), namely,

$$\mathcal{F}_N(\mathbf{q}) = i^N \psi_g(\mathbf{q}) \int_0^{2\pi} \frac{d\xi}{2\pi} \exp\{i[N\xi - \alpha\cos(\xi - \varphi) + \beta\sin(2\xi)]\}. \tag{33}$$

Using (33) in the case when the target is a hydrogenlike ion with nuclear charge Z, we receive

$$\mathcal{F}_N(\mathbf{q}) = i^N \sqrt{\frac{Z^3}{\pi}} \frac{4Z}{(q^2 + Z^2)^2} \times \int_0^{2\pi} d\xi \exp\{i[N\xi - \alpha\cos(\xi - \varphi) + \beta\sin(2\xi)]\}. \tag{34}$$

If the laser field is circularly polarized then, in accordance with (31), $\beta = 0$ and Eq. (34) acquires the form [cf. Eq. (24)]

$$\mathcal{F}_N(\mathbf{q}) = \sqrt{\frac{Z^3}{\pi}} \frac{8\pi Z}{(q^2 + Z^2)^2} e^{iN\varphi} J_N(\alpha). \tag{35}$$

4. The case of (20)

Using Eq. (20) in the S matrix (4), the FDCS reads

$$\frac{d^4\sigma^{\pm}}{dE_s dE_e d\Omega_s d\Omega_e} = \sum_{N=-\infty}^{\infty} d^3\sigma_N^{\pm} \delta\left(E_s + E_e - E_0 - E_g - \frac{\Delta}{2} \pm \frac{\Omega}{2} + N\omega\right), \tag{36}$$

where the momentum profile has the form

$$d^3\sigma_N^{\pm} = \frac{p_s p_e}{(2\pi)^3 p_0} \left(\frac{d\sigma}{d\Omega}\right)_{ee} |\mathcal{F}_N^{\pm}(\mathbf{q})|^2, \tag{37}$$

with

$$\mathcal{F}_N^{\pm}(\mathbf{q}) = e^{iN\varphi}\sqrt{\frac{|\Delta|+\Omega}{2\Omega}}\left(J_N(\alpha)\psi_g(\mathbf{q}) \mp e^{i\varphi}J_{N+1}(\alpha)\sum_{\nu}\frac{2\mathcal{M}_{f_\nu,g}}{|\Delta|+\Omega}\psi_{f_\nu}(\mathbf{q})\right). \quad (38)$$

If the target is a hydrogenlike ion with nuclear charge Z, then $f_\nu = 2p_m$ ($m = 0,\pm 1$) and according to (38) we arrive at

$$\mathcal{F}_N^{\pm}(\mathbf{q}) = e^{iN\varphi}\sqrt{\frac{|\Delta|+\Omega}{2\Omega}}\sqrt{\frac{Z^3}{\pi}}\frac{8\pi Z}{(q^2+Z^2)^2} \times\left[J_N(\alpha) \mp \left(\frac{2}{3}\right)^5\frac{2\alpha\omega^2}{|\Delta|+\Omega}\frac{(q^2+Z^2)^2}{\left(q^2+\frac{Z^2}{4}\right)^3}J_{N+1}(\alpha)\right], \quad (39)$$

where the generalized Rabi frequency is given by

$$\Omega = \sqrt{\Delta^2 + \left(\frac{8}{9}\right)^5\frac{\omega_{21}^2}{\omega^2}\frac{\mathcal{E}_0^2}{Z^2}}.$$

III. RESULTS AND DISCUSSION

In this section, we present and analyze the results of numerical calculations of the momentum profiles for the laser-assisted $(e,2e)$ process in symmetric noncoplanar EMS kinematics (see, for instance, Ref. [2]). In this kinematics, the scattered and ejected electron angles with respect to the incident electron direction are $\theta_s = \theta_e = 45^\circ$, the incident electron energy is $E_0 = 2$ keV $- E_g$, and the scattered and ejected electron energies are $E_s = E_e = E$. As a target we consider atomic hydrogen ($Z = 1$, $E_g = -0.5$ a.u.). The TDCS is studied as a function of q which is varied by scanning the out-of-plane azimuthal angle of the ejected electron ϕ_e. We examine such a range of q values that in the absence of the laser field the effects of distortion of the plane waves and the second Born effects are negligible [3]. Thus, one can safely neglect these effects in the presence of the laser field as well.

In the case of linear polarization (LP), we inspect the following two orientations of the laser electric field: $\boldsymbol{\mathcal{E}} \parallel \mathbf{p}_0$ (LP1) and $\boldsymbol{\mathcal{E}} \parallel \boldsymbol{\zeta}$ (LP2), where $\boldsymbol{\zeta} = [\mathbf{p}_0 \times \mathbf{p}_s]$. In the case of circular polarization (CP), the following two orientations of the laser wave vector are inspected: $\mathbf{k} \parallel \boldsymbol{\zeta}$ (CP1) and $\mathbf{k} \parallel \mathbf{p}_0$ (CP2). Note that below the Cartesian components of $\mathbf{q}$ refer to the coordinate system determined by the laser wave and polarization vectors as specified in Sec. II A.

A. Low-frequency regime

We choose the parameters of the laser field to be the same as those of the Nd-doped yttrium aluminum garnet laser utilized in the pioneering laser-assisted $(e,2e)$ measurements [12]: the photon energy is $\omega = 1.17$ eV and the intensity is $I = 4 \times 10^{12}$ W/cm^2. The laser frequency is well below the $1s \to 2p$ transition frequency $\omega_{21} = 10.2$ eV and the electric-field amplitude $\mathcal{E}_0 \approx 10^{-2}$ a.u. is much weaker than the typical field in the hydrogen atom, $\mathcal{E}_\mathrm{H} \sim 1$ a.u.

Three perturbation models for the field-dressed state of atomic hydrogen are involved in the present calculations, namely, those given by Eqs. (12), (14), and (15). Note that, for a given number of photons exchanged between the colliding system and the laser field, the value of the final electron energy E within model (12) is shifted from that within models (14) and (15) by a half of the ponderomotive energy (29). For the present choice of the laser parameters the energy shift is about 0.21 eV. Due to the energy shift the minimal value of q, which is realized in the in-plane geometry ($\phi_e = 0$), within model (12) is also shifted from that within models (14) and (15). The momentum shift is about 2.5×10^{-3} a.u. if $N \leqslant 2$ and therefore is insignificant for the analysis carried out below.

Figures 1–4 present the numerical results for the momentum profiles corresponding to the collision geometries specified above and different numbers of photons emitted or absorbed by the electron-hydrogen system. The magnitude of TDCS is largest when $N = 0$ and falls substantially with increasing the number of exchange photons, and such behavior is true not only for the $|N| \leqslant 2$ but also for the $|N| > 2$ processes, which are not shown in Figs. 1–4 as being superfluous for the purposes of the present analysis. This observation is readily explained by the fact that the laser field is weak and is far off the resonant regime—the probability of multiphoton processes rapidly decreases when the number of involved photons increases.

In Figs. 1 and 3, the momentum profiles for $N = 0$ within all three models of the field-dressed hydrogen state are close to the field-free momentum profile. The reason is that the latter is, up to a kinematical factor, determined by the $1s$ momentum density $|\psi_{1s}(\mathbf{q})|^2$ while the former by approximately $|J_0(\alpha)\psi_{1s}(\mathbf{q})|^2$. The argument of the zero-order Bessel function is constant (in the LP1 geometry) or practically constant (in the CP1 geometry) and its value is $\alpha \approx 0.2$, and hence $J_0(\alpha) \approx 1$ [24].

In contrast to Figs. 1 and 3, the laser-assisted momentum profiles for $N = 0$ displayed in Figs. 2 and 4 markedly differ from the field-free result. The observed difference is due to the Bessel function $J_0(\alpha)$, whose argument is estimated as $\alpha \approx 5.4 \times q$ in the LP2 case and $\alpha \approx 3.8 \times q$ in the CP2 case and hence, in contrast with the LP1 and CP1 cases, it varies in a wide range when the azimuthal electron angle ϕ_e is scanned. The oscillations in the laser-assisted momentum profiles observed in Figs. 2 and 4 can be attributed to the Bessel functions $J_N(\alpha)$. This conclusion is supported by the fact that the nodes in the momentum profiles coincide with the nodes of the Bessel functions. Since $J_{-N}(\alpha) = (-1)^N J_N(\alpha)$ [24], the oscillating structures for N and $-N$ are similar. Another difference as compared with the LP1 and CP1 cases is that the magnitude of the TDCS in the LP2 and CP2 geometries decreases more slowly when increasing the number of exchange photons. Our calculations show that this relatively slow decrease extends to the $|N| > 2$ results, which, as was already noted, are not presented here.

Let us analyze the dependence of the momentum profiles on the model for the field-dressed hydrogen state. All three

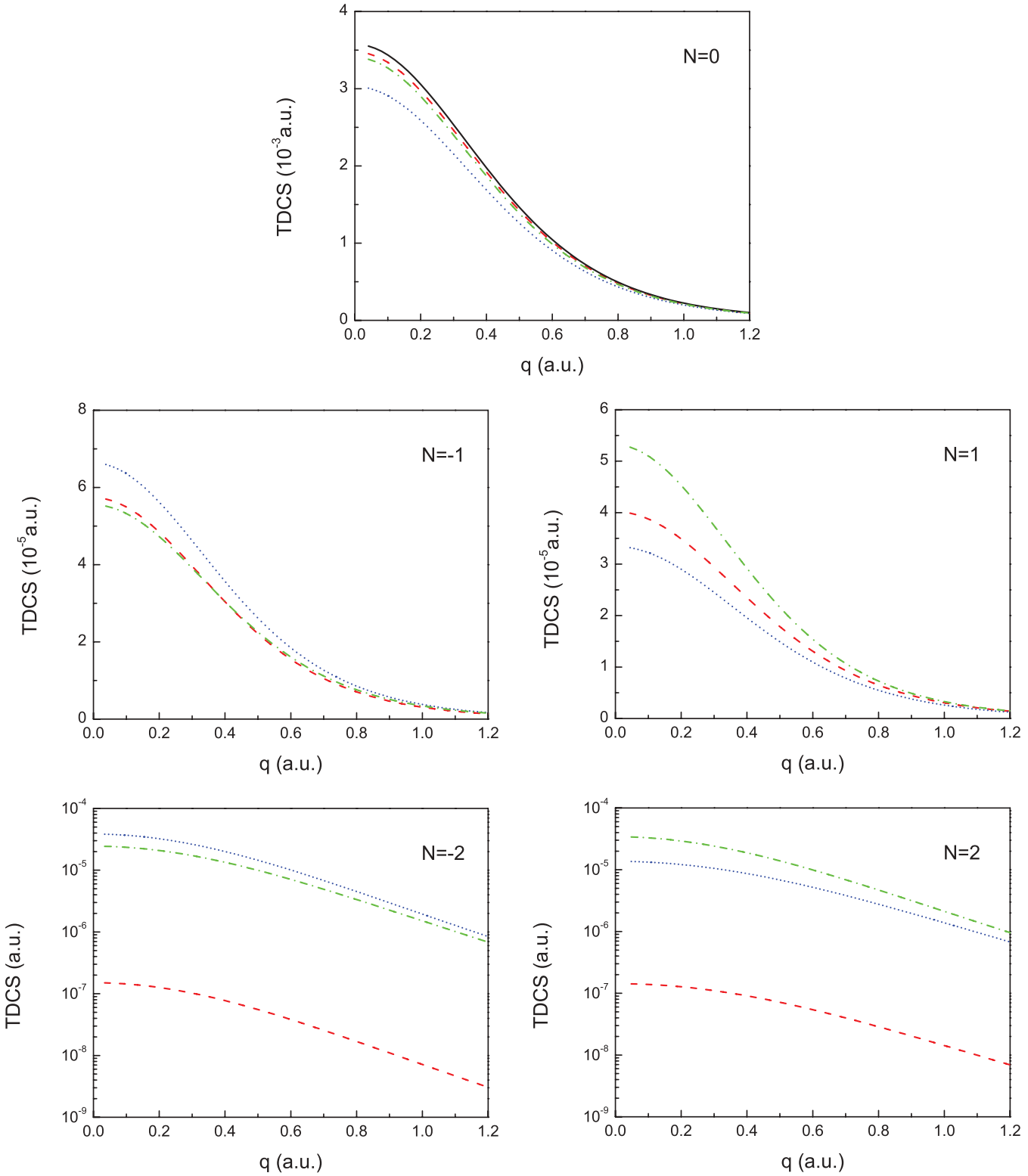

FIG. 1. (Color online) Noncoplanar symmetric momentum profiles in the LP1 geometry. When $N = 0$, solid curve shows the result in the absence of a laser field. Dashed curve corresponds to Eq. (12), dotted curve to Eq. (14), and dash-dotted curve to Eq. (15).

considered models yield more or less the same order of magnitude for the TDCS, excepting the case of LP1 geometry when $N = \pm 2$ (see Fig. 1). Specifically, in that particular case, the TDCS using model (12) is two orders of magnitude smaller than those using models (14) and (15). This finding can be attributed to the role played by the parameter β [see Eq. (31)] in Eqs. (32) and (34). As can be seen, this parameter is absent in Eq. (24). Moreover, in the CP1 geometry (Fig. 3), which

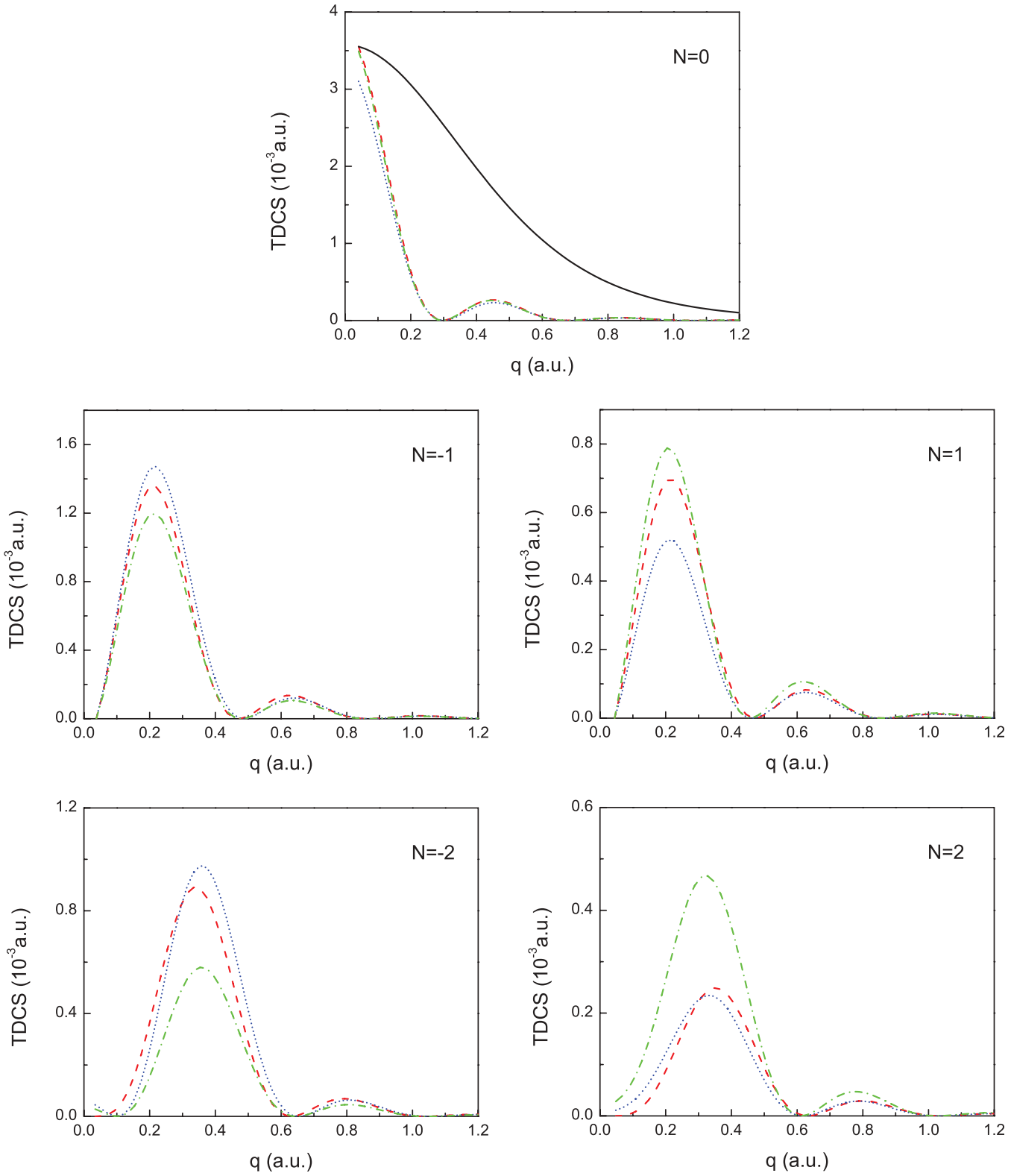

FIG. 2. (Color online) The same as in Fig. 1 but in the LP2 geometry.

among the others inspected is physically most close to the LP1 one, there is no such remarkable difference between the models when $N = \pm 2$ because $\beta = 0$ in this case.

As follows from the results presented in Figs. 1–4, when using the models (12) and (14) the photon absorption processes ($N < 0$) dominate those of photon emission ($N > 0$). This means that the system tends to absorb net energy from the radiation background. In contrast, when using the field-free hydrogen state (15) the photon emission processes are on a par with or even dominate those of photon absorption. This feature

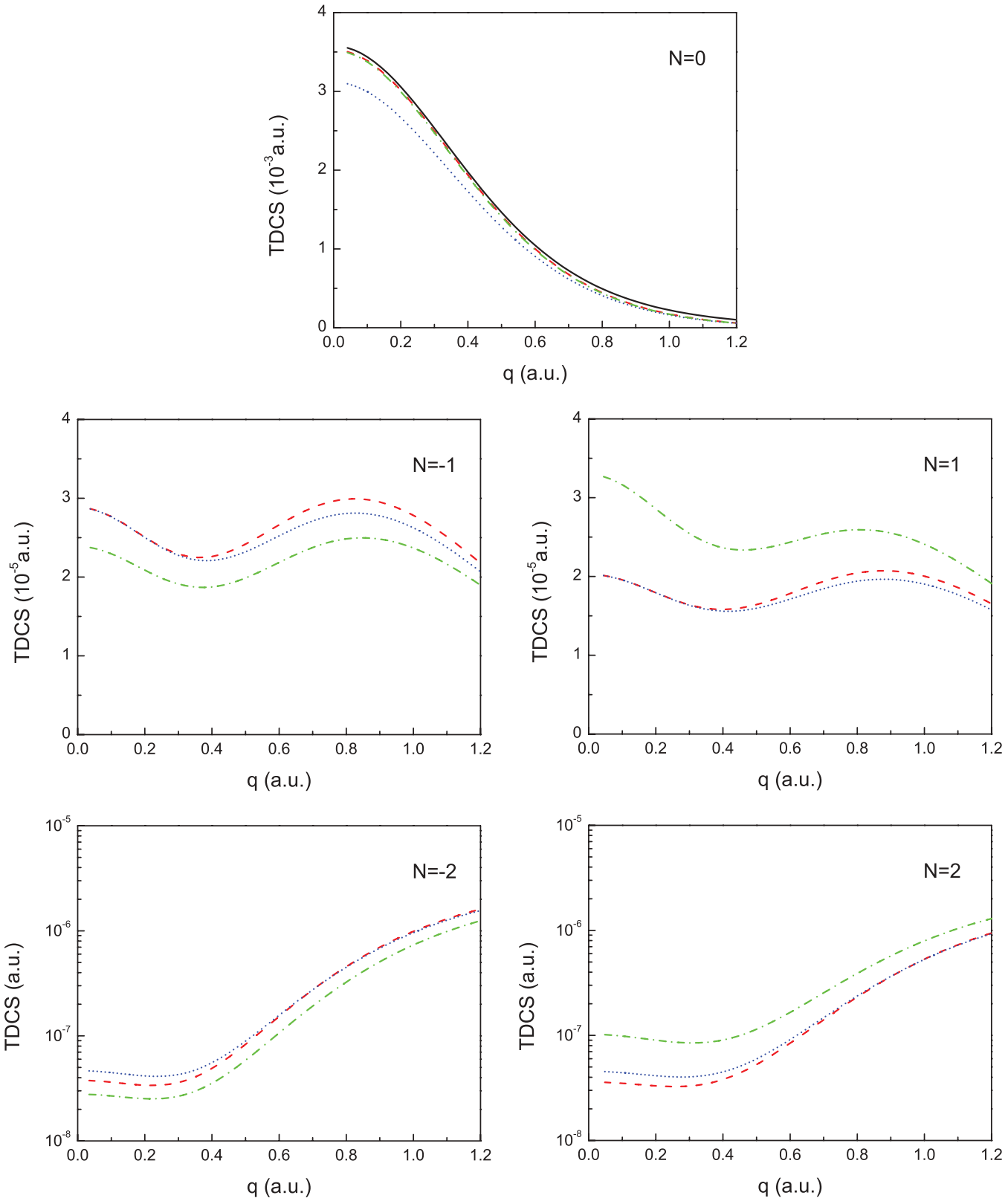

FIG. 3. (Color online) The same as in Fig. 1 but in the CP1 geometry.

indicates that it is the hydrogen atom that tends to absorb net energy from the radiation background.

As a general observation, the momentum profiles are rather sensitive to the perturbation treatment of the laser dressing of the hydrogen state. The sensitivity, however, depends on the number of exchange photons. For example, when $N = 0$, the results using models (12) and (15) are practically indistinguishable, especially in the CP1 and CP2 cases. The

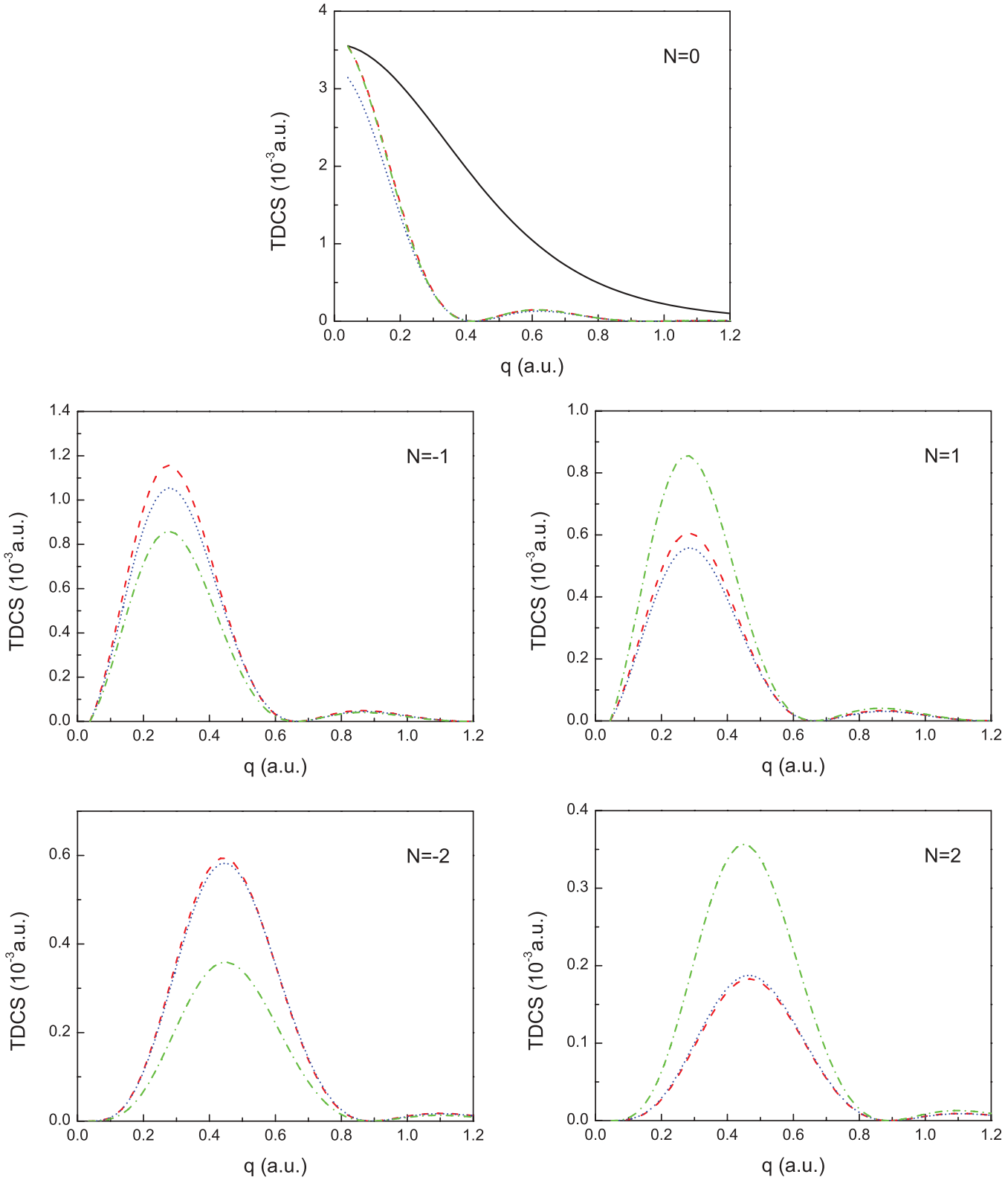

FIG. 4. (Color online) The same as in Fig. 1 but in the CP2 geometry.

reason is that Eqs. (24) and (35) are identical for $N = 0$. The sensitivity also depends on whether the laser field is linearly or circularly polarized. For example, the differences between the results using the field-dressed states (12) and (14) are more pronounced for the linearly polarized field, that is, in the LP1 and LP2 geometries.

B. Resonant regime

The laser frequency is resonant to the $1s \rightarrow 2p$ hydrogen transitions and the laser electric-field amplitude is taken as $\mathcal{E}_0 = 10^{-4}$ a.u. The laser pulse duration is assumed to be such that $T \ll \Gamma^{-1}$, where Γ is the width of the $2p$ state due to spontaneous emission and photoionization. This ensures that the populations of the $1s$ and $2p$ states are governed by the solution (17). Taking into account the present choice of the laser-field strength, we thus obtain the condition $T \ll 10^{-10}$ s. At the same time, T must be long on an atomic scale ($\sim 10^{-17}$ s) and much longer than the electron-electron collision duration ($\sim 10^{-17}$–10^{-16} s). Another important restriction is that the laser pulse turn on and off time δT must be much longer than the time necessary for the dressed state (20) to be built. The latter can be roughly estimated as the inverse Rabi frequency $1/\chi_{2p,1s}$. For $\mathcal{E}_0 = 10^{-4}$ a.u. we have $\chi_{2p,1s} \simeq 7.45 \times 10^{-5}$ a.u. and hence $\delta T \gg 10^{-13}$ s.

Figures 5–8 present the numerical results for the momentum profiles corresponding to different collision geometries and values of the reduced resonance detuning parameter $\eta = \Delta/\chi_{2p,1s}$. The results are shown only for the cases of no photon exchange ($N = 0$) and one-photon absorption ($N = -1$). For other cases ($N \neq 0, -1$) the absolute values of the momentum profiles are orders of magnitude smaller due to the weakness of the field and the nonresonant character of the relevant multiphoton processes. In other words, the free electrons' coupling to the laser field introduces very minor corrections as compared to the field-free situation; and what really matters is the resonant dressing of the hydrogen atom.

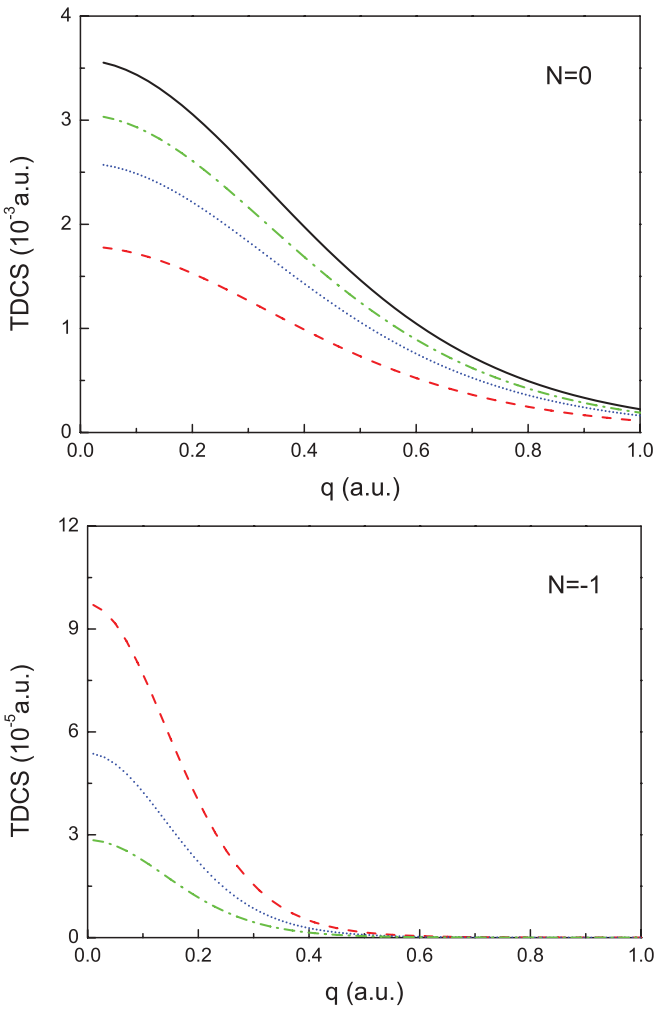

FIG. 5. (Color online) Noncoplanar symmetric momentum profiles in the LP1 geometry. When $N = 0$, solid curve shows the result in the absence of a laser field. Dashed curve corresponds to $\eta = 0$, dotted curve to $\eta = 0.5$, and dash-dotted curve to $\eta = 1$.

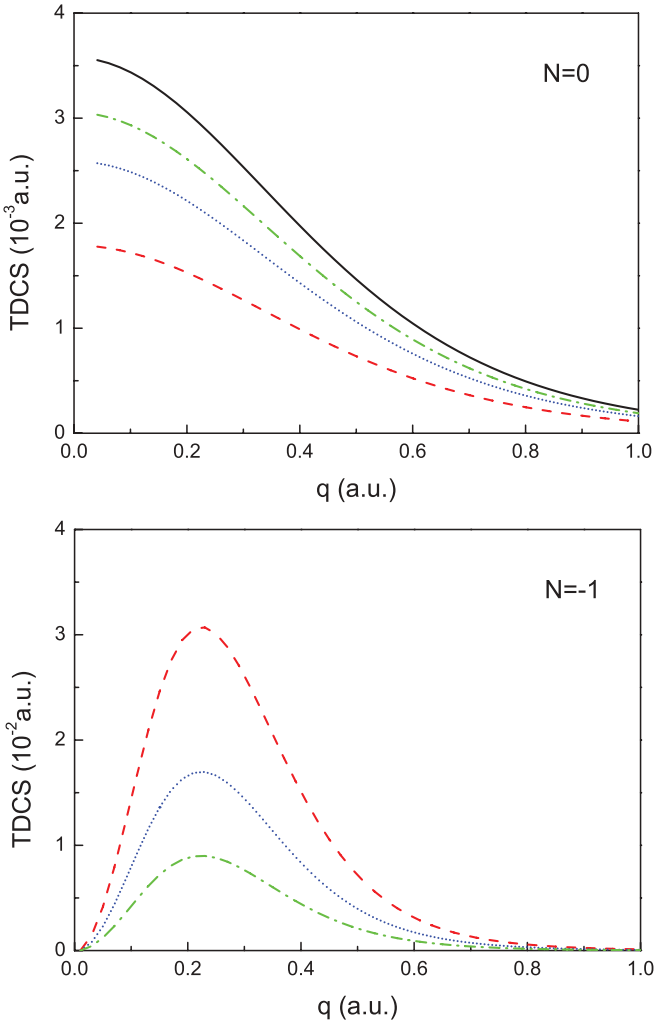

FIG. 6. (Color online) The same as in Fig. 5 but in the LP2 geometry.

It can be seen that the results for $N = 0$ are practically insensitive to collision geometry. The origin of this feature lies in the properties of Eq. (39). For the present set of laser parameters and collision geometries the value of the argument of the Bessel functions occurring in Eq. (39) is $\alpha < 10^{-3}$. Therefore one can use the following approximate expressions [24]:

$$J_{N\geqslant 0}(\alpha) = \frac{1}{N!}\left(\frac{\alpha}{2}\right)^N, \quad J_{N<0}(\alpha) = \frac{(-1)^{|N|}}{|N|!}\left(\frac{\alpha}{2}\right)^{|N|}.$$

According to these estimates, for $N = 0$ the contribution to Eq. (39) from the term containing $J_1(\alpha)$ is strongly suppressed and hence the momentum profile is almost fully determined by (up to a kinematical factor) $|a_{1s}|^2|\psi_{1s}(\mathbf{q})|^2$, where the

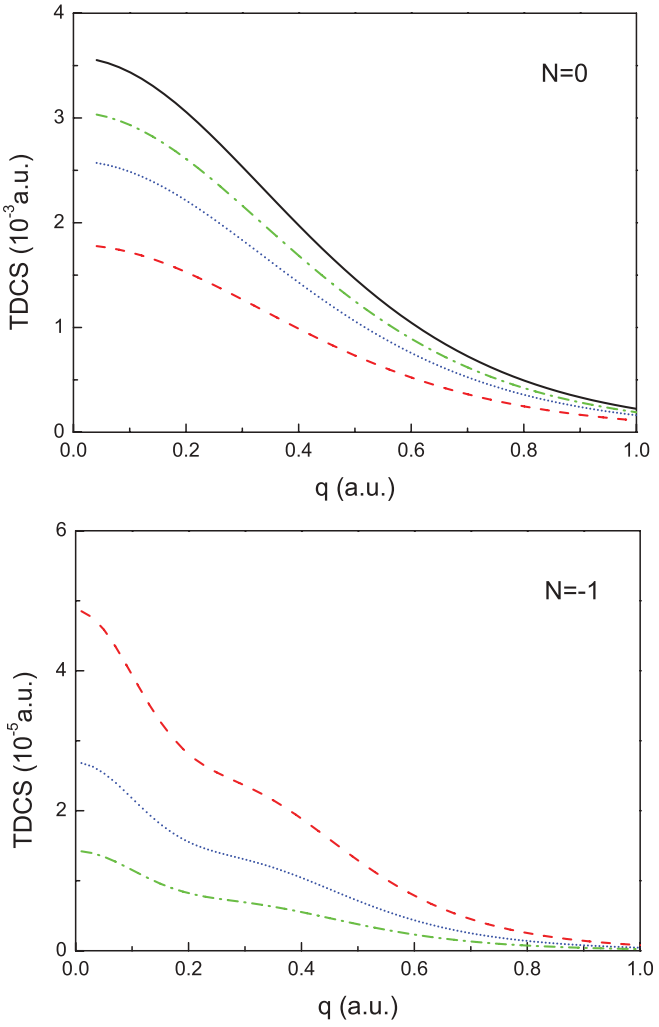

FIG. 7. (Color online) The same as in Fig. 5 but in the CP1 geometry.

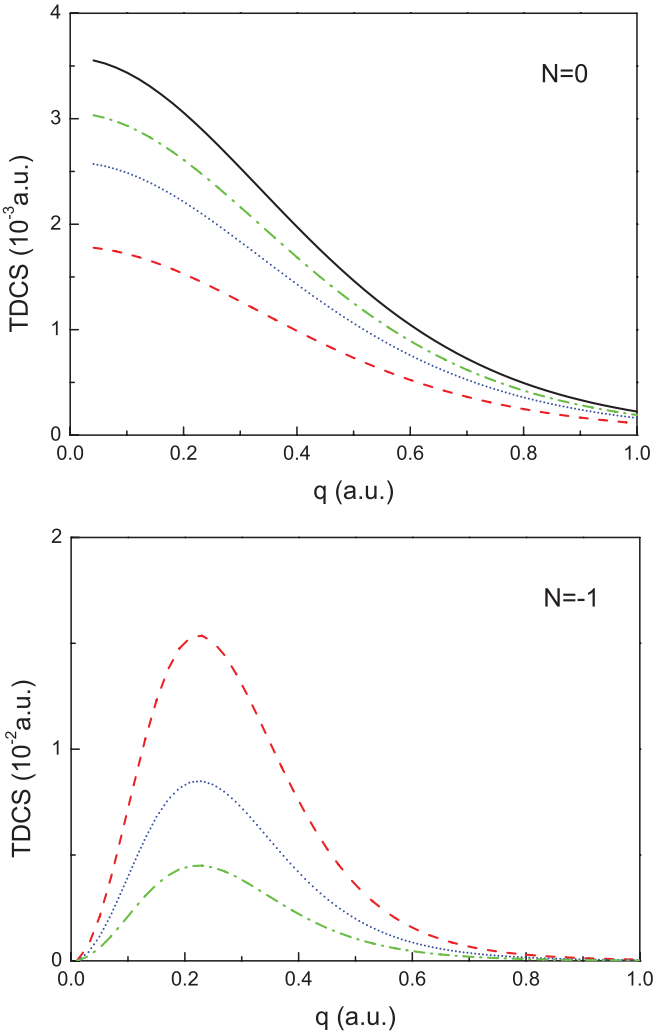

FIG. 8. (Color online) The same as in Fig. 5 but in the CP2 geometry.

population of the $1s$ state $|a_{1s}|^2$ (see Table I) does not depend on collision geometry.

In contrast to the case of no photon exchange, the results for $N=-1$ exhibit a strong dependence on collision geometry. The consideration analogous to that in the case $N=0$ yields that the momentum profile for $N=-1$ is determined by (up to a kinematical factor) $|a_{2p}|^2|\psi_{2p}(\mathbf{q})|^2$, where the population of the $2p$ state $|a_{2p}|^2$ (see Table I) does not depend on collision geometry but the momentum density $|\psi_{2p}(\mathbf{q})|^2$ of the ionized $2p$ orbital does. Usually in EMS studies one deals with unpolarized atomic targets. This means that one measures the momentum profile spherically averaged over directions of $\mathbf{q}$ (see, for instance, Ref. [9]). In the present situation, however, the laser electric field polarizes the target state and the direction of $\mathbf{q}$ becomes important. According to Eq. (17), the polarized $2p$ state is given by the mixture of the $2p_{+1}$ and $2p_{-1}$ states. In the LP case, one has

$$\left|\psi_{2p}^{\mathrm{LP}}(\mathbf{q})\right|^2 = \frac{8\pi q_x^2}{\left(q^2+\frac{1}{4}\right)^6}, \tag{40}$$

which means that the momentum density is maximal (zero) when $\mathbf{q}$ is parallel (perpendicular) to the laser polarization vector. In the LP1 geometry (Fig. 5), the value of q_x does not vary and equals to the minimal value of q ($q_{\min}=0.01$ a.u.). Therefore the shape of the $N=-1$ momentum profile depends only on the denominator in (40). In the LP2 geometry (Fig. 6), the absolute value of q_x varies in a wide range starting from zero. This explains why the $N=-1$ momentum profiles in this case are orders of magnitude larger and have different shapes than those in the LP1 geometry. Moreover, in sharp contrast to the LP1 case, the momentum profiles for $N=-1$ are appreciably larger in magnitude than those for $N=0$, notifying that in the LP2 geometry the EMS processes from the polarized $2p$ state dominate those from the

TABLE I. The values of populations of the $1s$ and $2p$ states, $|a_{1s}|^2$ and $|a_{2p}|^2$, calculated in accordance with RWA (17) as functions of the reduced resonance detuning parameter η.

η	$\lvert a_{1s}\rvert^2$	$\lvert a_{2p}\rvert^2$
0	0.5	0.5
0.5	0.7236	0.2764
1	0.8536	0.1464

$1s$ state. In particular, the maximal value of the momentum profile for $N=-1$ is an order of magnitude larger than that for $N=0$ when the exact resonance ($\eta=0$) is realized and, according to Table I, the $1s$ and $2p$ states are equally populated. This result conforms with the fact that an electron in the $2p$ state is less bound and hence it is easier to knock out than that in the $1s$ state. In the CP case, one has

$$\left|\psi_{2p}^{\mathrm{CP}}(\mathbf{q})\right|^2=\frac{4\pi\left(q_x^2+q_y^2\right)}{\left(q^2+\frac{1}{4}\right)^6}, \tag{41}$$

which means that the momentum density reaches its maximal value in the plane perpendicular to the laser wave vector $\mathbf{k}$. The CP1 and CP2 cases can be analyzed in a similar manner as the LP1 and LP2 ones. Without loss of generality we suppose that the x axis is parallel to $\mathbf{p}_0$. Then in the CP1 geometry (Fig. 7) the value of q_x is the same as in the LP1 case ($q_x=0.01$ a.u.) and the value of q_y ranges from 0 (when $q=0$) to approximately 0.08 a.u. (when $q=1$ a.u.). Thus, in accordance with a comparison of Eqs. (40) and (41), at $q\sim 0$ the CP1 momentum profile for $N=-1$ is twice smaller in magnitude than the respective LP1 one, whereas at larger values of q it is comparable to or even exceeds the LP1 one in magnitude. In the CP2 geometry (Fig. 8), the value of q_x varies in the same range as in the LP2 case and the absolute q_y value is given by $q_y\simeq q_x^2/(2\sqrt{E})\approx 0.08q_x^2$. Therefore, q_y plays an unimportant role in (41) and the CP2 momentum profile for $N=-1$ is given by simply the respective LP2 one scaled by a factor of $1/2$.

The behavior of the momentum profile with respect to the reduced resonance detuning parameter η can be readily understood from the above analysis and Table I. Namely, in the case of exact resonance ($\eta=0$) the absolute value of the momentum profile for $N=0$ is minimal while that for $N=-1$ is maximal. With increasing (decreasing) η the $N=0$ momentum profile scales up (down) in the same way as does the $1s$ population $|a_{1s}|^2$ while the $N=-1$ momentum profile scales down (up) in the same way as does the $2p$ population $|a_{2p}|^2=1-|a_{1s}|^2$. Note that, following (19), $|a_{1s}|^2=|a_{2p}|^2=0.5$ when $\eta=0$ and $|a_{1s}|^2>0.5$, $|a_{2p}|^2<0.5$ when $\eta\neq 0$. Another remark is that for not too large values of $|\eta|$ the cases of η and $-\eta$ are practically indistinguishable. This reflects the smallness of the generalized Rabi frequency Ω, which thus very slightly affects the value of the final electron energy E, and the smallness of α discussed above, which makes the terms describing interference of the $1s$ and $2p$ contributions [$\propto J_N(\alpha)J_{N+1}(\alpha)$] to the TDCS negligible.

IV. SUMMARY AND CONCLUSIONS

In summary, we have delivered a theoretical analysis of the EMS of an atomic system in the presence of laser radiation with the electric field amplitude being much smaller than the intra-atomic field. By analogy to the PWBA in the field-free case, the Volkov wave Born approximation has been formulated for evaluation of the laser-assisted momentum profiles. This approximation accounts for laser modification of plane waves, which traditionally describe the incoming and outgoing electron states of the EMS method in the absence of external fields. To assess the potential of EMS for studying the field-dressed target states, several dressing mechanisms depending on the laser frequency have been involved in the present analysis. Numerical calculations of the momentum profiles assisted by few-photon emission or absorption have been carried out in the case of atomic hydrogen embedded in a background laser field of linear or circular polarization. The results exhibited notable dependencies on collision geometry, number of transferred photons, and the dressing of the atomic state.

For the low-frequency, nonresonant laser field, we have found that the dressing of the atomic state even only to first order of time-dependent perturbation theory crucially influences the laser-assisted momentum profiles. Moreover, different versions of the first-order perturbation approach have different effect on the results. These findings reflect a rich potential of the laser-assisted EMS for elucidating the dressing mechanism even in such situations where the laser-field effect on the target states is considered to be far from being strong. In the resonant regime, even a very weak laser field can efficiently couple the ground and excited target states. And our analysis shows that this coupling can characteristically manifest itself in the laser-assisted momentum profiles. Namely, one observes typical EMS momentum profiles from the ground and excited states, populations of which depend on laser parameters. In addition, the momentum profile from the excited state directly reflects the laser polarization.

Some comments should be made regarding possible realization of the EMS measurements in the presence of a resonant laser field. Presently no laser sources exist which operate at the frequency resonant to the $1s\rightarrow 2p$ transition in atomic hydrogen. More suitable candidates for the target in this respect would be the alkali-metal-like atoms or ions, for example, such as lithium and sodium atoms, where the energy separating the ground and first excited states is much smaller and thus the resonance condition for these states can be achieved with available lasers. Note that similar qualitative effects as those determined in this work can be expected for such more complex atomic systems.

Finally, it is useful to draw a parallel between the laser-assisted EMS and so-called $(\gamma,e\gamma)$ spectroscopy, which is based on x-ray Compton scattering, for both methods provide the same information about the target electron state in the field-free situation (see, for instance, Ref. [9]). First theoretical considerations of the laser-assisted Compton scattering were undertaken in Ref. [25]. There it was found that even a relatively weak laser field seriously modifies the Compton profile compared to the field-free case, in which it is given by the projection of the momentum density on the direction of momentum transfer. Recently, theoretical calculations of the FDCS for Compton scattering in the presence of laser radiation were reported in Ref. [26]. Only energy spectra of the scattered photons and recoil electrons were examined there. At the same time, it would be interesting to investigate the laser-field effect on the momentum distributions, similarly to what has been done in this work.

ACKNOWLEDGMENTS

We are grateful to Dmitri Eremenko and Maarten Vos for useful discussions.

[1] Yu. F. Smirnov and V. G. Neudachin, JETP Lett. **3**, 192 (1966).

[2] N. Watanabe, Y. Khajuria, M. Takahashi, Y. Udagawa, P. S. Vinitsky, Yu. V. Popov, O. Chuluunbaatar, and K. A. Kouzakov, Phys. Rev. A **72**, 032705 (2005).

[3] N. Watanabe, M. Takahashi, Y. Udagawa, K. A. Kouzakov, and Yu. V. Popov, Phys. Rev. A **75**, 052701 (2007).

[4] Z. H. Luo, C. G. Ning, K. Liu, Y. R. Huang, and J. K. Deng, J. Phys. B **42**, 165205 (2009); Z. J. Li, X. J. Chen, X. Shan, T. Liu, and K. Z. Xu, J. Chem. Phys. **130**, 054302 (2009); B. Hajgató, M. S. Deleuze, and F. Morini, J. Phys. Chem. A **113**, 7138 (2009).

[5] K. L. Nixon, W. D. Lawrance, D. B. Jones, P. Euripidies, S. Saha, F. Wang, and M. J. Brunger, Chem. Phys. Lett. **451**, 18 (2008).

[6] C. Chen, M. N. Gale, A. S. Kheifets, M. Vos, and M. R. Went, J. Phys.: Condens. Matter **17**, 7689 (2005); M. Vos, C. Bowles, A. S. Kheifets, and M. R. Went, Phys. Rev. B **73**, 085207 (2006); K. L. Nixon, M. Vos, C. Bowles, and M. J. Ford, Surf. Interface Anal. **38**, 1236 (2006).

[7] M. A. Coplan, J. H. Moore, and J. P. Doering, Rev. Mod. Phys. **66**, 985 (1994).

[8] V. G. Neudatchin, Yu. V. Popov, and Yu. F. Smirnov, Phys. Usp. **42**, 1017 (1999).

[9] E. Weigold and I. E. McCarthy, *Electron Momentum Spectroscopy* (Kluwer Academic/Plenum, New York, 1999).

[10] M. Takahashi, Bull. Chem. Soc. Jpn. **82**, 751 (2009).

[11] K. A. Kouzakov, P. S. Vinitsky, Yu. V. Popov, and C. Dal Cappello, J. Electron Spectrosc. **161**, 35 (2007); V. L. Shablov, P. S. Vinitsky, Yu. V. Popov, O. Chuluunbaatar, and K. A. Kouzakov, Phys. Part. Nuclei **41**, 335 (2010).

[12] C. Höhr, A. Dorn, B. Najjari, D. Fischer, C. D. Schroter, and J. Ullrich, Phys. Rev. Lett. **94**, 153201 (2005); J. Electron Spectrosc. **161**, 172 (2007).

[13] M. H. Mittleman, *Introduction to the Theory of Laser-Atom Interaction* (Plenum, New York, 1993).

[14] P. Francken and C. J. Joachain, J. Opt. Soc. Am. B **7**, 554 (1990).

[15] F. Ehlotzky, A. Jaroń, and J. Z. Kamiński, Phys. Rep. **297**, 63 (1998); F. Ehlotzky, *ibid.* **345**, 175 (2001).

[16] D. M. Volkov, Z. Phys. **94**, 250 (1935); W. Gordon, *ibid.* **40**, 117 (1926).

[17] M. V. Fedorov, *Atomic and Free Electrons in a Strong Light Field* (World Scientific, Singapore, 1997).

[18] S.-M. Li, J. Berakdar, S.-T. Zhang, and J. Chen, J. Phys. B **38**, 1291 (2005); J. Electron Spectrosc. **161**, 188 (2007).

[19] S.-M. Li, J. Chen, and Z.-F. Zhou, Eur. Phys. J. D **7**, 39 (1999).

[20] C. J. Joachain, P. Francken, A. Maquet, P. Martin, and V. Veniard, Phys. Rev. Lett. **61**, 165 (1988); P. Martin, V. Veniard, A. Maquet, P. Francken, and C. J. Joachain, Phys. Rev. A **39**, 6178 (1989).

[21] D. Khalil, A. Maquet, R. Taïb, C. J. Joachain, and A. Makhoute, Phys. Rev. A **56**, 4918 (1997); A. Makhoute, D. Khalil, A. Maquet, and R. Taïeb, J. Phys. B **32**, 3255 (1999).

[22] A. B. Voitkiv and J. Ullrich, J. Phys. B **34**, 1673 (2001).

[23] P. Cavaliere, G. Ferrante, and C. Leone, J. Phys. B: At. Mol. Phys. **13**, 4495 (1980); P. Cavaliere, C. Leone, R. Zangara, and G. Ferrante, Phys. Rev. A **24**, 910 (1981).

[24] *Handbook of Mathematical Functions with Formulas, Graphs, and Mathematical Tables*, edited by Milton Abramowitz and Irene A. Stegun (Dover, New York, 1972).

[25] F. Ehlotzky, Opt. Commun. **25**, 221 (1978); Phys. Lett. A **69**, 24 (1978); M. Jain and N. Tzoar, Phys. Rev. A **18**, 538 (1978).

[26] A. B. Voitkiv, N. Grün, and J. Ullrich, J. Phys. B **36**, 1907 (2003); **37**, 2641 (2004).